




Review

$\delta^{34}\text{S}$, $\delta^{18}\text{O}$, and $\delta^2\text{H}$ - $\delta^{18}\text{O}$ as an Approach for Settling the Question of Groundwater Salinization in Neogene Basins: The North of Morocco in Focus

Mohammed Elgettafi ^{1,*}, Malak Elmeknassi ^{2,3}, Abdenabi Elmandour ⁴, Mahjoub Himi ^{5,6}, Juan M. Lorenzo ⁷ and Albert Casas ⁶

- ¹ Polydisciplinary Faculty of Nador, Géo-Environnement et Santé, Mohamed I University, Oujda, LCM2E Lab BP 300, Selouane 62702, Morocco
 - ² Geology & Sustainable Mining Institute (GSMI), Mohamed VI Polytechnic University, Ben Guerir 43150, Morocco
 - ³ Center for Remote Sensing Applications (CRSA), Mohamed VI Polytechnic University, Ben Guerir 43150, Morocco
 - ⁴ Mohamed VI Museum for the Civilization of Water in Morocco, Ministry of Habous and Islamic Affairs, Marrakesh 40000, Morocco
 - ⁵ GEE, Laboratory of Applied Sciences (LSA), ENSAH, Abdelmalek Essaadi University, Al Hociema 32003, Morocco
 - ⁶ Earth Sciences Faculty, University of Barcelona, Martí i Franquès, s/n, 08028 Barcelona, Spain
 - ⁷ Department of Geology and Geophysics, Louisiana State University, Baton Rouge, LA 70802, USA
- * Correspondence: m.elgettafi@ump.ac.ma



Citation: Elgettafi, M.; Elmeknassi, M.; Elmandour, A.; Himi, M.; Lorenzo, J.M.; Casas, A. $\delta^{34}\text{S}$, $\delta^{18}\text{O}$, and $\delta^2\text{H}$ - $\delta^{18}\text{O}$ as an Approach for Settling the Question of Groundwater Salinization in Neogene Basins: The North of Morocco in Focus. *Water* **2022**, *14*, 3404. <https://doi.org/10.3390/w14213404>

Academic Editor: Xiaohu Wen

Received: 24 September 2022

Accepted: 24 October 2022

Published: 27 October 2022

Publisher's Note: MDPI stays neutral with regard to jurisdictional claims in published maps and institutional affiliations.



Copyright: © 2022 by the authors. Licensee MDPI, Basel, Switzerland. This article is an open access article distributed under the terms and conditions of the Creative Commons Attribution (CC BY) license (<https://creativecommons.org/licenses/by/4.0/>).

Abstract: Neogene plains around the Mediterranean basin are characterized by considerable groundwater salinization. Some studies have misidentified seawater intrusion as the main source of salinity. Across northern Morocco, we gathered $\delta^{18}\text{O}_{\text{SO}_4}$ and $\delta^{34}\text{S}_{\text{SO}_4}$ data from coastal and inland aquifers, Messinian marls, and volcanic products. Differences in the isotopic composition between Messinian marls and some groundwater in all aquifer samples indicate that salinization in groundwater is a consequence of dissolution of Messinian evaporite deposits; nevertheless, modern agriculture and wastewater strongly influence depletion in levels of $\delta^{34}\text{S}_{\text{SO}_4}$. Our novel approach enables effective investigation of processes governing salinity in Neogene basins to support more informed water resource management and governance.

Keywords: Neogene basins; groundwater salinity; $\delta^{18}\text{O}_{\text{SO}_4}$; $\delta^{34}\text{S}_{\text{SO}_4}$; northern Morocco

1. Introduction

The perimeter of the Mediterranean basin has played a key role in cultural exchanges between its inhabitants in both east-to-west and north-to-south directions. Thanks to its history and favorable climate, the Mediterranean basin has seen and continues to experience a steady and significant population growth, strong urbanization, and increases in the level of groundwater consumption. In particular, Morocco, because of its geographic situation, has been considered to be a migration hub between dry northern Africa and the more humid central and northern Europe. Presently, Morocco handles and struggles with large increases in water demand. In this context, the Moroccan government has been engaged in a dynamic policy on water resource management and governance to provide the country with important hydraulic infrastructure, improve access to drinking water, and develop smart irrigation. In fact, groundwater is not just a prerequisite for life, but also an essential element for socioeconomic development. Groundwater quality and quantity in Morocco are directly impacted by human development [1], climate change [2], and the local geological environment [3]. These impacts have been noticed in the behavior and response of aquifers to reduced precipitation, increased groundwater pumping [4],

and pollution [5,6]. The sources of groundwater salinity in Morocco include seawater intrusion [7], dissolution of evaporites in Neogene basins [8], Triassic sediments [9], and agricultural irrigation [10]. This paper reviews the current state of isotope analyses which combine the most novel isotopic signatures in groundwater, with their interpretation in terms of Messinian-aged marls and volcanic products. The latter contain ancient and unique isotopic sulfur compositions and thus serve to assess the possible sources of sulfate ions in groundwater. We chose to analyze Messinian marls and volcanic pyroclastic rocks because marls commonly form the substratum of the aquifers in northern Morocco, and during the Messinian period explosive volcanic eruptions were widespread. This volcanic activity appears in the form of many pyroclastic flows and cinerites within the sedimentary series. Although most Messinian evaporite deposits have been eroded, and it is difficult to find suitable outcrops for sampling, we consider that Messinian volcanism may have affected the geochemical composition of similar-aged sediments as well as marls.

In this paper, we use isotopic and geological analyses to suggest a novel interpretation for the origin of groundwater salinization. Based on prior hydrochemical studies in these areas, two working hypotheses have been proposed. The first suggests that there is a likely mixing of freshwater with seawater in coastal aquifers [6,10], and the second interprets an enrichment of groundwater by Cl^- , Na^+ , SO_4^{2-} , Ca^{2+} and Mg^{2+} [11] from geological sources. Our objective is to address some critical questions concerning groundwater salinity in northern Morocco: (1) Do sediments dating from the Messinian Salinity Crisis (MSC; from 5.96 to 5.33) play a role in triggering the mineralization of groundwater, or (2) is groundwater mineralization caused by saltwater intrusion from the Mediterranean Sea? In this regard, we describe the geochemical features which characterize groundwater in Neogene basins in northern Morocco and establish how the stratigraphic record of the MSC relates to the different proposed groundwater salinization scenarios across the whole Mediterranean basin perimeter? To help answer these questions, (1) we present a geological synthesis of MSC in the Mediterranean basin, (2) hydrogeochemical and isotopic analyses of groundwater samples whose origin of mineralization is in question and (3) perform a comparison of isotopic data collected from the Ghis-Nekor, BouAreg-Gareb and Kert aquifers in northern Morocco, whose mineralization comes exclusively from interaction with Messinian marls, cinerites and a mixture of marls cinerites deposits.

2. Regional Geology

Between the Tortonian and the Holocene, the geological history of the Moroccan Rif area (Figure 1) was dominated by the tectono-sedimentary evolution of the Riffian belt, controlled by both the westward motion of the Alboran microplate and the northward displacement of Africa with respect to Europe [12]. The Rif Mountains area resulted from complex nappe sequences from that period. From the Upper Miocene (Messinian) until the Quaternary [13], intra mountainous basins continued to develop and deform. However, the distinct event that marked the region during this period was the Messinian Salinity Crisis (MSC). The MSC corresponds to the break of connection between the Atlantic Ocean and the Mediterranean Sea, causing the desiccation of the Mediterranean Sea [14]. Consequently, thick evaporitic units were deposited in the Mediterranean [15], as well as in the marginal basins [16]. Marginal and deep basin evaporites are chronologically disconnected by as much as 260 kyr [17]. That is because the Mediterranean Sea and Atlantic Ocean probably continued to be partially connected via Riffian and Betic Corridors in the north of Morocco and in the south of Spain, respectively. Until recently, two principal causes of the MSC were proposed, including a break in communication between the Atlantic and the Mediterranean Sea caused by plate tectonics [18,19], combined with global climatic and eustatic changes [20,21]. The absolute age of the MSC is still a cause of geological debate. There is general common agreement on the age of the start of the salinity crisis (5.96 Ma) and its end at 5.33 Ma [22], with duration of 0.63 Ma. Nonetheless, some still suggest that the MSC began at about 5.7 Ma, and ended at about 5.3 Ma; with duration of about 0.4 Ma [23].

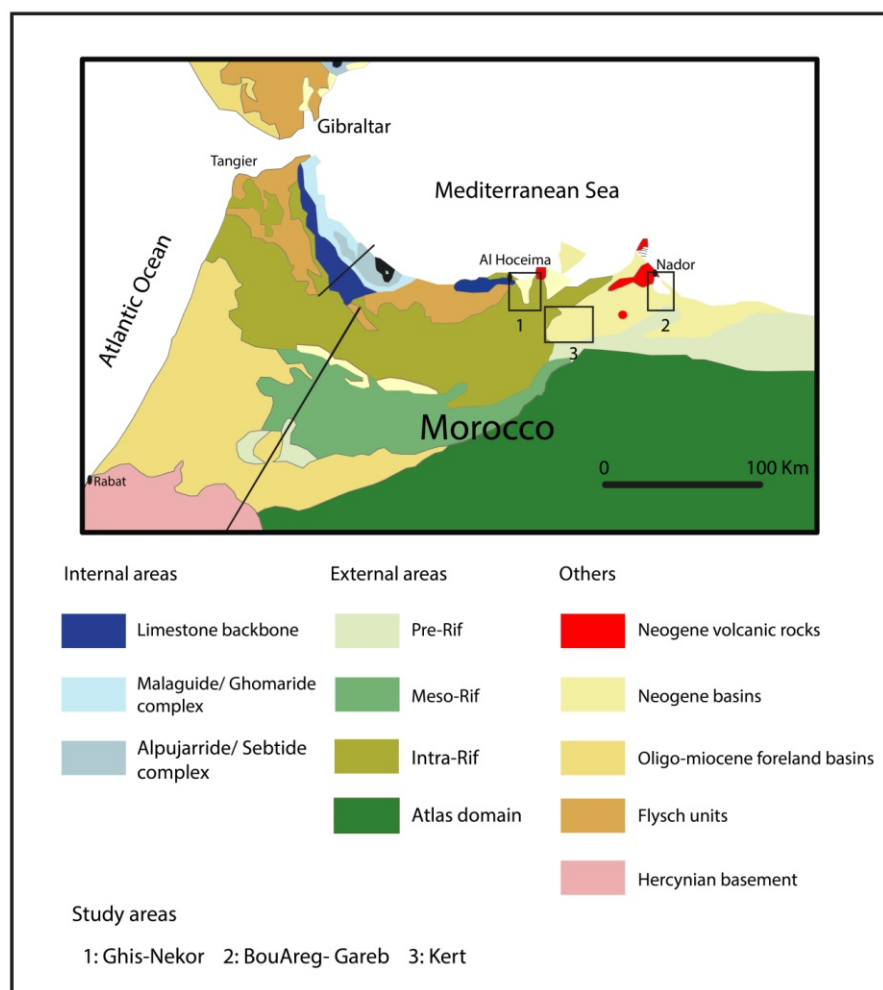


Figure 1. Geological map of Rif ranges and Neogene basins [24].

2.1. Local Geology and Hydrogeology

2.1.1. Ghis-Nekor Plain

The Ghis-Nekor Plain of the Al Hoceima region is located between the Internal and External Zones of the Rif Mountains. Volcanic rocks of the Tortonian–Messinian outcrop in Ras Tarf, east of Al Hoceima [25] and Neogene Plio-Quaternary sediments are confined to the Ghis-Nekor basin. This latter is bounded by Bousekkour–Aghbal and Trougout onshore faults, extending offshore to the Mediterranean Sea. The Bokkoya fault (Figure 2a,b) is a major eastward dipping fault that bounds the western Al Hoceima Bay [26]. The Trougout fault represents the active eastern major fault of the Nekor strike–slip related basin, while the Bousekkour–Aghbal and Bokkoya faults were recently active along its diffuse western boundary. Between these structures, small fault-bounded sub-basins connect at depth to a steep WSW dipping master fault, all together forming a large-scale transtensional basin with an interpreted “flower structure” at depth (Figure 2b) [26]. Previous studies [10] show that transmissivity in the Ghis-Nekor aquifer varies between $8.8 \times 10^{-4} \text{ m}^2\text{s}^{-1}$ and $6.5 \times 10^{-2} \text{ m}^2\text{s}^{-1}$. The maximum values are observed around the Nekor and Ghis Rivers, while the lowest values are located in the eastern part, ranging between 3.75 and $0.6 \times 10^{-3} \text{ m}^2\text{s}^{-1}$. The permeability values vary in the range of 10^{-3} to $3 \times 10^{-6} \text{ ms}^{-1}$. In fact, the majority of the aquifer is characterized by permeability values higher than $0.1 \times 10^{-3} \text{ ms}^{-1}$, while the lowest values are observed in the eastern plain where hydraulic permeability is less than $0.001 \times 10^{-3} \text{ ms}^{-1}$.

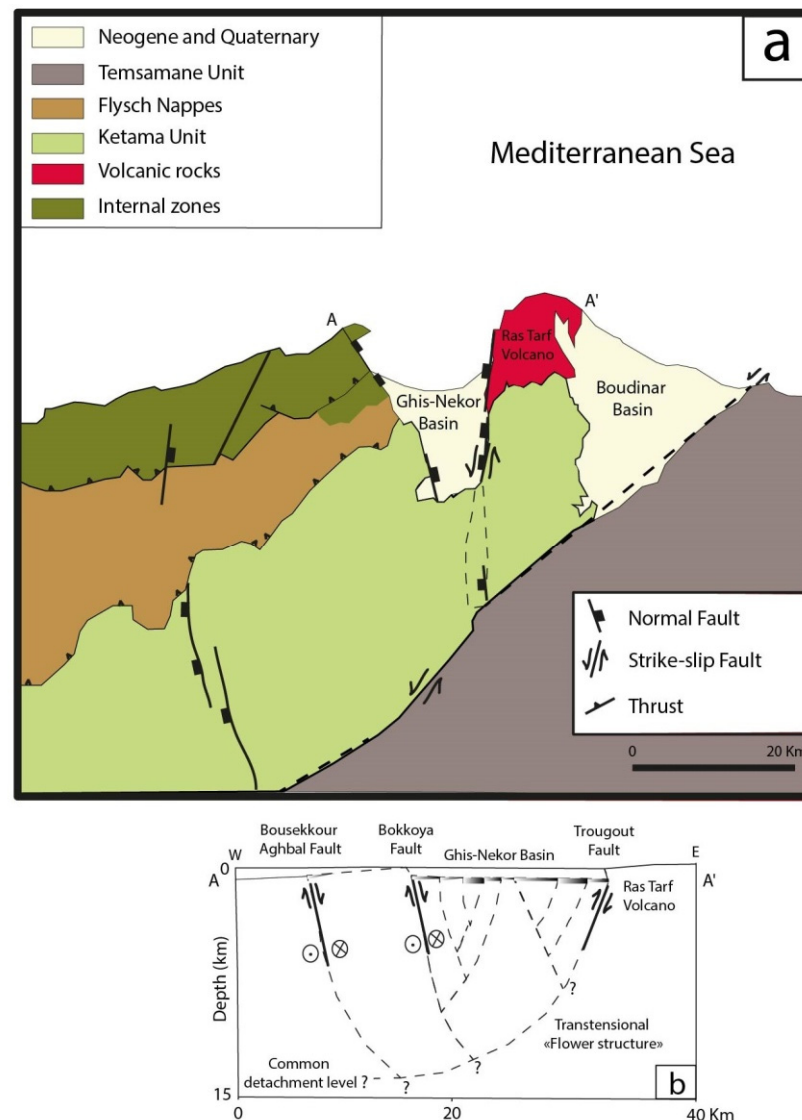


Figure 2. Geological map of the Al Hoceima region (a) [27–29]. E–W structural cross-section AA' (b) [26].

2.1.2. BouAreg-Gareb Plain

The BouAreg-Gareb study area is located within the Neogene basin of the Melilla-Nador region, where there are two aquifers. The coastal aquifer lies beneath the BouAreg plain and the continental one beneath the Gareb plain. These two aquifers are hydrogeologically connected across the Selouane passage (Figure 3). From a combined hydrogeological point of view, the BouAreg and Gareb aquifers cover an area of about 480 km². The aquifers lie within Plio-Quaternary deposits and are bounded at their base by a Neogene substratum of marls. The aquifers have good hydrodynamic characteristics [30], mainly associated with high permeability ($7 \times 10^{-4} \text{ ms}^{-1}$) in the vicinity of the lagoon (Sebkha) to the west, while the lowest values are found at the borders of the Kibdana massif. Transmissivity varies continuously from upstream ($9 \times 10^{-4} \text{ m}^2\text{s}^{-1}$) to the coastal zone ($2 \times 10^{-2} \text{ m}^2\text{s}^{-1}$). The highest values for transmissivity are found in the west, whereas the lowest are measured at the borders of the Kibdana massif, probably due to the accumulation of marls. All along the coast, the transmissivity ranges around $2 \times 10^{-2} \text{ m}^2\text{s}^{-1}$ [31].

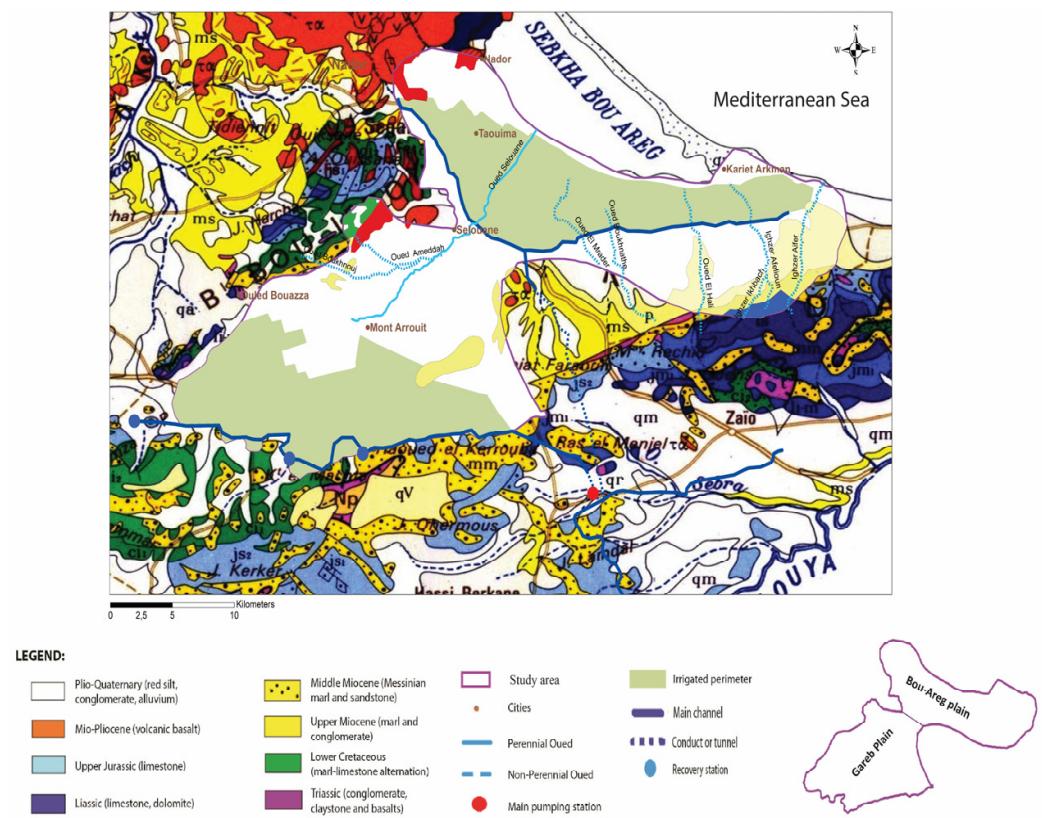


Figure 3. Geological map of the BouAreg and Gareb plains.

2.1.3. Kert Plain

The Kert basin, which covers a total area of about 250 km², is located in northeastern Morocco (Figure 4A). During the Miocene to Villafranchian, the Kert depression received mixed and varied thick marine and continental sediments. We consider that the Miocene deposits contain gypsum as can be seen in some outcrops of the region. At its top, the series ends with gravels, silts, and clays from the Villafranchian age. The Plain of Kert (Figure 4) is limited to the east by the western Gareb range. The metamorphic massif of Tamsamane which limits the plain in the north and northwest was affected by a compressive tectonic event generating a N120°E fracture cleavage associated with green schists [32]. The southern portion of the basin contains Intra-Riffain nappes and Miocene marls. Further south, the plain is surrounded by mostly Jurassic and Cretaceous carbonates rocks. The strata of key hydrogeological formations can be identified (Figure 4B). The substratum of the aquifer is represented by Upper Miocene transgressive marls, which are overlain by the Plio-Quaternary deposits comprising limestones and conglomerates.

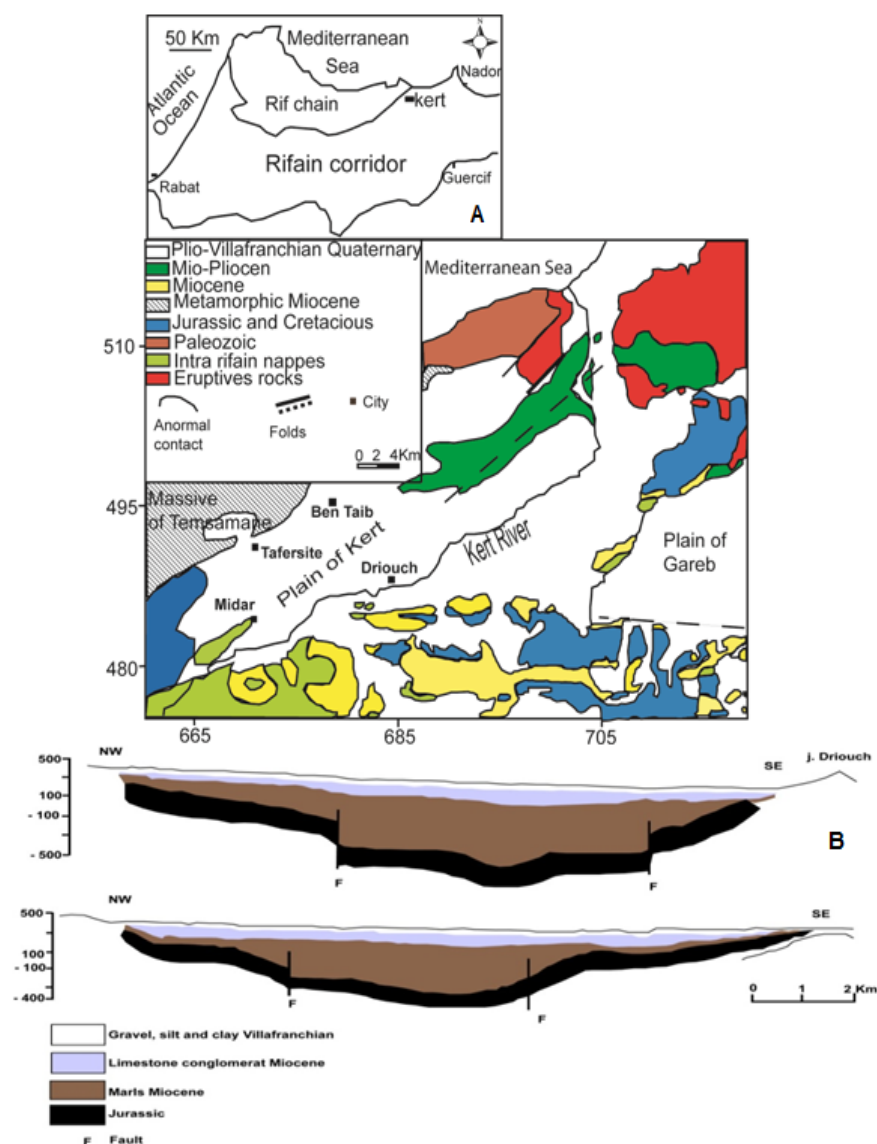


Figure 4. Geological sketch (A) and Hydrogeological cross-section of the Kert Plain(B) [33]. (modified from [34].

3. Materials and Methods

For our research, the $\delta^2\text{H}$ and $\delta^{18}\text{O}$ of water were obtained by H_2 and CO_2 equilibrium, respectively, and isotope ratio mass spectrometry (IRMS) was conducted with a Delta-S Finnigan Mat Mass Spectrometer. For S and O isotope analysis, the dissolved SO_4 was precipitated as BaSO_4 by the addition of $\text{BaCl}_2 \cdot 2\text{H}_2\text{O}$, after acidifying the sample with HCl and boiling it to prevent $\text{Ba}(\text{CO}_3)$ precipitation. The S isotopic composition was determined with an Elemental Analyzer (Carlo Erba 1108) coupled with an IRMS (Delta-C Finnigan Mat). The O isotopic composition was analyzed with a thermo-chemical elemental analyzer (TC/EA Thermo-Quest Finnigan) coupled with an IRMS (Delta-C Finnigan Mat). Notation is expressed in terms of $\delta\%$ relative to Vienna Standard Mean Ocean Water (V-SMOW) and Vienna Cañón Diablo Troilite (V-CDT) standards. The isotope ratios were calculated using international and internal laboratory standards. The reproducibility of the samples calculated from standards systematically interspersed in the analytical batches is $\pm 0.5\%$ for $\delta^2\text{H}$, $\pm 0.2\%$ for $\delta^{18}\text{O}_{\text{H}_2\text{O}}$, $\pm 0.2\%$ for $\delta^{34}\text{S}$, and $\pm 0.5\%$ for $\delta^{18}\text{O}_{\text{SO}_4}$. All water samples for isotopic analyses were prepared and analyzed at the Scientific-Technical Services of the University of Barcelona. Isotopes of Messinian marls and volcanic deposits were prepared and analyzed at the Oxy-Anion Stable Isotope Consortium of the Louisiana State University.

4. Results and Discussion

4.1. $\delta^{18}\text{O}$ and $\delta^2\text{H}$

Isotopic analyses ($\delta^{18}\text{O}$ and $\delta^2\text{H}$) were conducted on groundwater samples collected from productive wells and rivers. The distribution of the well and river samples is given in Figure 5, and the isotopic analyses of these samples are presented in Table 1. The $\delta^{18}\text{O}$ and $\delta^2\text{H}$ collected from the Ghis-Nekor aquifer vary from -5.37‰ to -4.15‰ and from -41.7‰ to -28.4‰ respectively. Nearly all sample data plot below the Global Meteoric Water Line (GMWL) [35] (Figure 5). This river’s water isotopic contents are 6.2‰ for $\delta^{18}\text{O}$ and 40.5‰ for $\delta^2\text{H}$ and plot almost on the GMWL. Notably, we interpret that sample analyses from Ghis-Nekor aquifer plot along two evaporation lines. The first sample, taken from a well at the eastern edge of the aquifer and with a source whose composition ($\delta^2\text{H}$: 34.40‰ ; $\delta^{18}\text{O}$: -5.63‰) is marked by the intersection of the (upper) evaporation line and the GWML. The second evaporation line (from the west) connects relatively freshwater sample data of the Ghis River whose signature is more depleted in heavy isotopes. Samples taken from wells located progressively further north samples show greater enrichment in heavy isotopes. Between these two evaporation lines lie data taken from samples in intermediate wells, corresponding to cases of mixed groundwater.

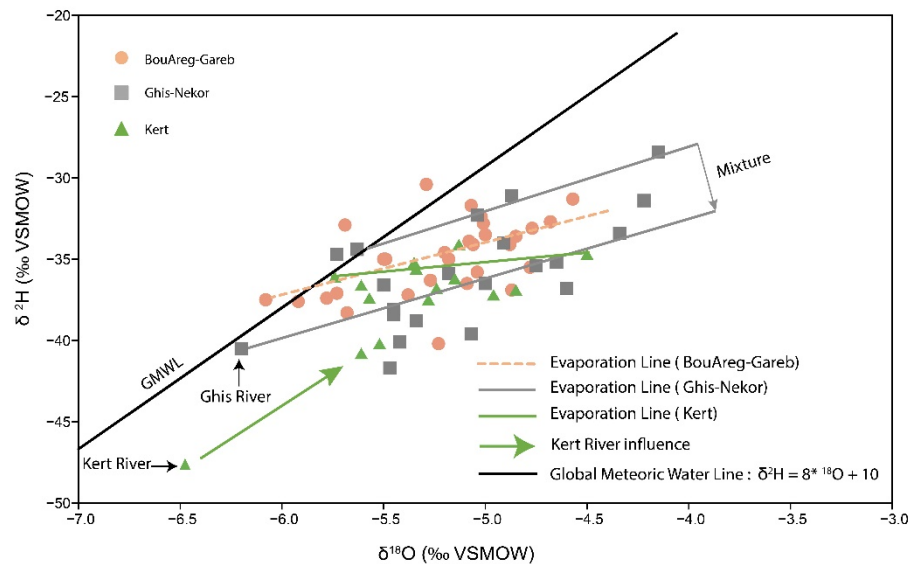


Figure 5. Isotope $\delta^2\text{H}$ – $\delta^{18}\text{O}$ compositions of the groundwater in the study areas.

Table 1. Isotopes analysis ($\delta^{18}\text{O}$, $\delta^2\text{H}$ and $\delta^{34}\text{S}_{\text{SO}_4}$ and $\delta^{18}\text{O}_{\text{SO}_4}$), chemical analysis (sodium, chloride, sulfate, and nitrate) and electrical conductivity. S: Spring, R: Well near manure, GR: Ghis River, KR: Kert River, MM: Messinian Marls, C: Cinerite and VMD: volcanic marls deposits.

ID	EC	Na ⁺	Cl ⁻	SO ₄	NO ₃ ⁻	$\delta^{18}\text{O}_{\text{H}_2\text{O}}$	$\delta^2\text{H}$	$\delta^{18}\text{O}_{\text{SO}_4}$	$\delta^{34}\text{S}$	Slope
	$\mu\text{S}/\text{cm}$	mg/L				‰				
B1	2010	431	802	102	6	-6.08	-37.5	5.75	15.5	7.81
B2	3840	851	1385	342	35	-5.38	-37.2	9.24	14.9	8.78
B4	6210	1507	2490	324	14	-5.29	-30.4	6.51	17.0	7.63
B5	6670	1219	2428	339	34	-5.01	-32.8	6.24	6.4	8.56
B10	6880	1473	2344	472	34	-5.68	-38.3	7.13	12.2	8.51
B15	6070	984	1448	594	25	-4.87	-36.9	8.30	14.6	9.62
B17	6910	1783	2286	490	15	-4.77	-33.1	8.76	15.4	9.03
B18	3430	523	748	602	30	-5.09	-36.5	8.36	12.0	9.13
B21	5160	1156	1590	771	32	-5.06	-34.1	9.93	12.0	8.71
B23	7840	346	398	538	28	-4.78	-35.5	8.83	9.1	9.52
B26	8300	935	2171	780	18	-5.23	-40.2	6.71	6.7	9.60

Table 1. Cont.

ID	EC	Na ⁺	Cl ⁻	SO ₄	NO ₃ ⁻	δ ¹⁸ O _{H₂O}	δ ² H	δ ¹⁸ O _{SO₄}	δ ³⁴ S	Slope
	μS/cm	mg/L					‰			
B27	6260	1337	1495	793	9	-4.68	-32.7	8.65	11.0	9.13
B29	5330	932	795	681	41	-5.27	-36.3	8.64	8.8	8.78
B31	22,600	2961	6759	810	5	-4.57	-31.3	11.08	14.5	9.03
B32	17,000	2875	5112	339	8	-5.50	-35.0	5.94	13.3	8.18
B33	4260	453	1068	579	62	-5.07	-31.7	6.80	12.5	8.22
B34	4900	1081	994	882	45	-5.00	-33.5	10.56	10.2	8.70
G1	6680	1783	2933	506	16	-5.20	-34.6	4.75	8.2	8.58
G3	11,900	2034	3050	546	16	-5.04	-35.8	5.79	7.0	9.08
G5	8040	1855	2627	866	27	-4.85	-33.6	7.35	9.9	8.98
G6	4890	1507	1988	779	32	-5.18	-35.0	8.54	9.6	8.67
G7	8055	1498	2370	879	39	-4.88	-34.1	8.38	9.9	9.03
G8	5660	955	1590	572	37	-5.73	-37.1	11.48	9.0	8.22
G9	5630	1070	1463	590	39	-5.78	-37.4	10.82	9.1	8.20
G10	3970	598	1022	603	8	-5.92	-37.6	7.39	2.7	8.05
G11	11,200	1679	3465	750	15	-5.08	-33.9	6.61	9.4	8.64
G13	4810	449	909	562	29	-5.02	-32.4	11.11	11.9	8.45
S	19,700	3197	5853	398	8	-5.49	-35.0	8.43	8.7	8.20
R	1680	276	298	235	62	-5.69	-32.9	5.79	9.9	7.53
GN3	2419	281	277	589	15	-5.47	-41.7	7.02	2.9	7.63
GN8	2859	277	414	621	15	-5.00	-36.5	6.89	3.6	7.30
GN9	4624	575	927	944	41	-4.34	-33.4	7.31	5.6	7.69
GN20	4000	527	646	755	46	-4.87	-31.1	4.41	1.3	6.39
GN23	5011	615	1063	407	123	-4.15	-28.4	7.57	7.5	6.84
GN27	4062	527	775	485	485	-5.04	-32.3	5.29	3.7	6.41
GN32	2561	204	333	561	9	-5.42	-40.1	4.72	-4.3	7.40
GN34	5958	759	1315	1031	10	-5.50	-36.6	8.40	1.7	6.65
GN37	5117	620	839	1267	41	-4.65	-35.2	6.90	3.2	7.57
GN39	2916	267	412	663	32	-5.45	-38.4	4.35	3.8	7.05
GN40	10,575	1497	2976	990	112	-4.22	-31.4	6.28	9.9	7.45
GN44	4008	472	548	1111	20	-5.07	-39.6	6.79	3.0	7.82
GN45	2796	255	362	725	16	-4.75	-35.4	7.13	3.5	7.45
GN46	3433	352	502	847	14	-5.34	-38.8	6.95	2.9	7.27
GN48	3357	346	509	840	17	-4.60	-36.8	7.94	3.4	8.00
GN49	4167	484	653	1101	11	-5.18	-35.9	8.60	4.0	6.94
GN50	2723	300	394	500	21	-5.73	-34.7	5.76	2.6	6.05
GN53	3400	376	558	522	30	-5.63	-34.4	4.88	2.2	6.11
GN57	6760	1208	1101	1615	42	-4.91	-34.0	7.17	4.5	6.92
GN59	2750	251	420	601	27	-5.45	-38.1	7.35	4.7	6.99
GR	2200	250	459	700	6	-6.20	-40.5	4.95	-4.4	6.53
K1	5670	822	1153	1397	66	-5.61	-36.6	7.21	0.0	6.52
K2	5050	843	122	666	35	-5.61	-40.8	8.03	6.1	7.25
K3	4680	792	974	639	30	-5.74	-36.1	8.76	7.2	6.28
K4	6990	1189	1867	1168	36	-4.96	-37.2	7.63	10.0	7.50
K5	7420	1658	1289	1462	0	-5.24	-36.8	13.86	16.0	7.00
K6	1330	149	243	107	27	-5.13	-34.1	7.77	3.5	6.63
K7	2830	581	458	248	12	-5.34	-35.6	5.02	5.6	6.65
K8	6200	886	1517	1316	96	-4.85	-36.9	6.31	-0.4	7.59
K9	3690	664	739	428	17	-5.15	-36.2	8.64	6.8	7.02
K10	5080	881	1064	1435	18	-5.35	-35.2	6.33	2.0	6.61
K11	850	55	86	134	18	-5.57	-37.4	5.79	-2.2	6.71
K12	1020	172	64	55	24	-5.52	-40.2	6.78	8.3	7.57
K13	4120	547	758	1063	94	-4.50	-34.7	8.21	-1.4	7.69
K14	4520	634	1121	512	65	-5.28	-37.5	6.54	8.7	7.08
KR	3828	3830	485	1476	21	-6.47	-47.6	5.30	-4.6	7.35
MM								6.43	18.3	
C								3.99	6.8	
VSD								6.56	17.6	

In the BouAreg-Gareb aquifer, $\delta^{18}\text{O}$ and $\delta^2\text{H}$ compositions of groundwater range from -6.1‰ to -5.2‰ and from -40.2‰ to -30.4‰ , respectively. All sample data plot either under or along the GMWL. This suggested that enrichment in heavy isotopes is typical for water that has been subjected to evaporation. If we consider the point of intersection between sample values and the GMWL, the inferred isotopic composition would be the source of recharge. This point has values of $\delta^2\text{H}$: -37.6‰ and $\delta^{18}\text{O}$: -6.08‰ and comes from a sample located near the Kebdana Mountains.

In the Kert aquifer the $\delta^{18}\text{O}$ and $\delta^2\text{H}$ compositions of groundwater range from -5.74 to -4.51‰ and from -40.8‰ to -34.1‰ , respectively. The surface water sample taken from the Kert River has values of -6.47‰ for $\delta^{18}\text{O}$, and -47.6‰ for $\delta^2\text{H}$. These values are more depleted in heavy isotopes compared to the groundwater, suggesting a high-altitude recharge. All the water well samples plot along an evaporation line (Figure 5) with an interpreted source whose composition ($\delta^2\text{H}$: -36.1‰ ; $\delta^{18}\text{O}$: -5.74‰) is given by the intersection of the evaporation line and the GMWL. A diffusion process could potentially exist between groundwater and Kert River (Figure 5).

Without absolute age dates it is difficult to estimate the recharge age of groundwater in the area studies. Nevertheless, the high concentration of NO_3^- (Table 1) in the groundwater can be attributed to present-day anthropogenic sources mainly from agriculture, animal manure and wastewater.

We note that both interior and coastal aquifers have a similar isotopic composition. Based on geographical position of wells and the intersection of the evaporation line with the GMWL, we suggest that aquifers are being recharged by runoff (Kert aquifer) and groundwater flow from the RasTraf (Ghis-Nekor aquifer) and Kebdana/Aroui Mountains (BouAreg-Gareb aquifer). All the data from groundwater samples show relatively low slopes, less than 8 (Table 1), although according to the conventional interpretation, this result may reflect slight and variable degrees of evaporation during or after rainfall infiltration under different climatic conditions. The low slopes indicate that the evaporation mechanism is not sufficient to explain the increasing salinity in all aquifers. In the following section, we use sulfur and oxygen isotopes of sulfate to resolve the question of groundwater salinity.

4.2. $\delta^{18}\text{O}_{\text{SO}_4}$ and $\delta^{18}\text{O}_{\text{H}_2\text{O}}$

For the Ghis-Nekor study area, isotopic measurements were performed on 20 groundwater samples from aquifer wells and a surface water sample from the Ghis River. The $\delta^{18}\text{O}$ isotopic content in sulfates (SO_4) varies between $+4.35\text{‰}$ and $+8.60\text{‰}$, while the isotopic signature of $\delta^{18}\text{O}$ in SO_4 from the Ghis river SO_4 is $+4.95\text{‰}$. In the BouAreg-Gareb study area, isotopic measurements were carried out on 29 well samples and one sample from the Al-Arouit spring. The oxygen isotope data for sulfates ($\delta^{18}\text{O}_{\text{SO}_4}$) in water samples range from $+4.75\text{‰}$ to $+11.48\text{‰}$, and is $+8.4\text{‰}$ in the Al-Arouit spring. The oxygen isotope data for sulfates ($\delta^{18}\text{O}_{\text{SO}_4}$) extracted from 14 water samples collected in the Kert aquifer vary from $+5.02\text{‰}$ to $+13.86\text{‰}$, and is $+5.3\text{‰}$ in Kert River (Table 1).

We suggest that the dominant control of $\delta^{18}\text{O}$ of in the groundwater comes from mixing with dissolved sulfate sediment, i.e., precipitated gypsum or anhydrite. Our data indicate that the $\delta^{18}\text{O}_{\text{SO}_4}$ values may be a function of the sulfate sources and not the water composition because otherwise, sulfates formed via sulfide oxidation would show a good correlation between $\delta^{18}\text{O}_{\text{SO}_4}$ and $\delta^{18}\text{O}_{\text{H}_2\text{O}}$, which is not observed (Figure 6). A key attribute of sulfate ions is that they do not exchange oxygen with the surrounding groundwater [36] and our sample values plot on a trend distinct from those of atmospheric O_2 . If either the groundwater or atmosphere had exerted a strong isotopic influence, the isotope sulfate data values would trend along or near either the 1:1 line or the atmospheric O_2 line (Figure 6), which they do not.

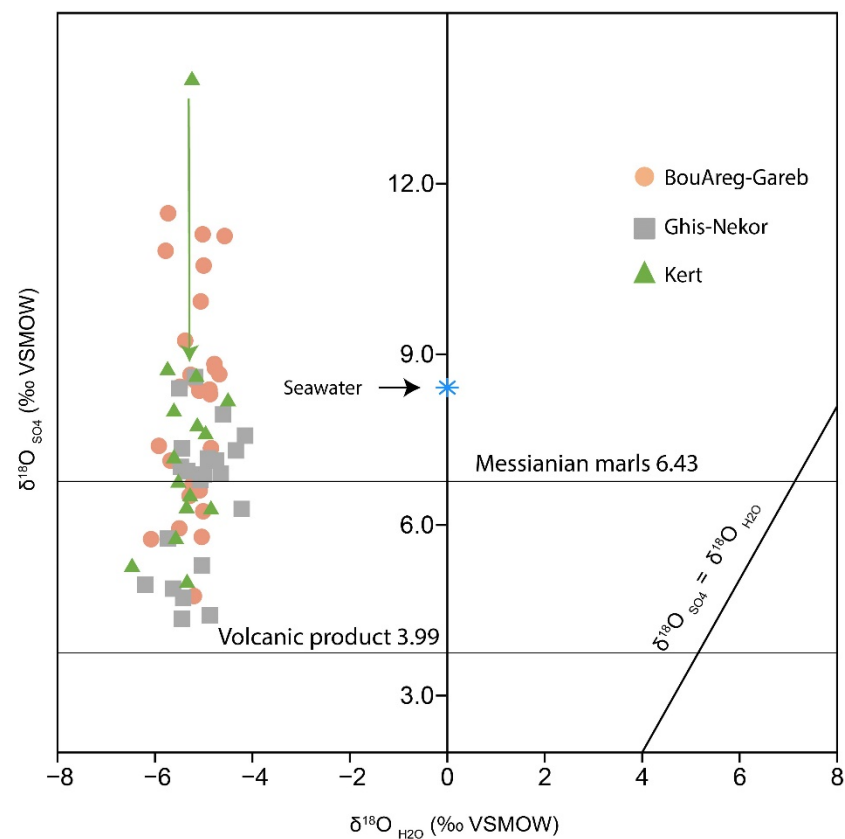


Figure 6. Oxygen isotope compositions of the dissolved sulfate species ($\delta^{18}\text{O}_{\text{SO}_4}$ versus) relative to those of groundwater ($\delta^{18}\text{O}_{\text{H}_2\text{O}}$) from which the sulfate was extracted seawater data from [37], O-O line from [38].

Similar to the Neogene basins in southern Spain, our data also show that the original seawater from which gypsum/anhydrite precipitated is also considerably lighter than regular seawater 8.6‰ [37]. Most of our sulfate samples show $\delta^{18}\text{O}$ values different to that expected for modern marine sulfates (8.6‰) or volcanic products (3.99‰), although the plotted sample values show a trend (Figure 6) toward that of volcanic products, indicating their geochemical influence. Together, $\delta^{18}\text{O}$ values and their trends taken from sulfate ions indicate that during the precipitation of evaporites in the Messinian the marginal basins were receiving an input of continental water influenced by volcanic products.

4.3. $\delta^{34}\text{S}_{\text{SO}_4}$ and $\delta^{18}\text{O}_{\text{SO}_4}$

Messinian marls and marls-volcanic deposits ($\delta^{34}\text{S} = 18.3\text{‰}$, $\delta^{18}\text{O}_{\text{H}_2\text{O}} = 6.43\text{‰}$, $^{34}\text{S} = 17.6\text{‰}$, $\delta^{18}\text{O}_{\text{H}_2\text{O}} = 6.56\text{‰}$) show no similar isotopic composition to actual seawater ($^{34}\text{S} \approx 20\text{‰}$, $\delta^{18}\text{O}_{\text{H}_2\text{O}} \approx 9.5\text{‰}$). Our data indicate that low values of $\delta^{34}\text{S}$ and $\delta^{18}\text{O}_{\text{H}_2\text{O}}$ in our Neogene basins are controlled mainly by continental water [39] or an additional supply of Triassic sulfates [40]. In our case (Figure 7), the decrease of isotopic values also implies that during the Messinian, marginal basins in the north of Morocco were isolated from Mediterranean Sea, or at least with a limited connection. Consequently, they were more influenced by continental waters enriched with light isotopes. Plotted $\delta^{34}\text{S}$ values from groundwater samples show no consistent relationship to the high concentration of SO_4 , $\delta^{18}\text{O}$ (Table 1) or the distance from the sea. However, the downward shift of $\delta^{34}\text{S}$ values to values below that of Messinian marls (EM: Figure 7) may be a consequence of some contamination. Considering the high concentrations measured for NO_3^- in groundwater, all aquifers are expected to show depletion in $\delta^{34}\text{S}$. The responsible anthropogenic contamination from animal manure concomitantly supplies sulfates rich in light sulfur. In addition, volcanic products can contribute light sulfur isotopes (EM₁: Figure 7), with a value of $\delta^{34}\text{S}$: 6.8‰

and so decrease the value of this isotopic signal. Furthermore, surface water (EM₂; Figure 7) plays an important role in changing the isotopic signature. In general, sulfates of non-gypsiferous origin dissolved either in surface water or, altered by volcanic products, are depleted in heavy isotopes. Based on the high amount of SO₄, we assume that although groundwater does not conserve the Messinian marls's (EM) isotopic signal, the salinity was originally derived from dissolution of gypsum concealed in Messinian marls. However, the change from the initial (EM) to final state is controlled by river water, agriculture, and volcanic products. This change, in contrast, relates only to the isotopic signal, and not to the salinity. The sulfate sources identified in this study is similar to those found in southern Spain [41].

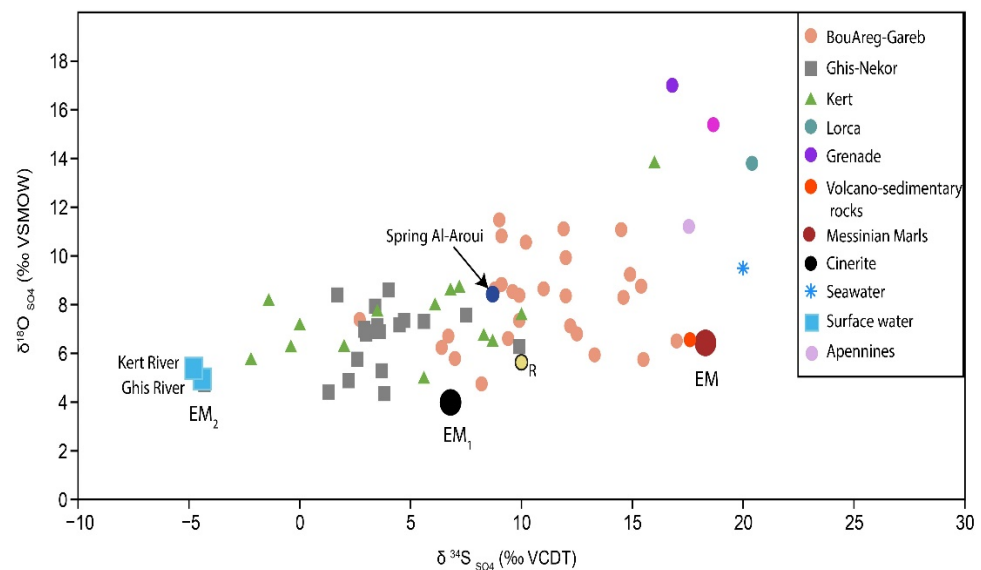


Figure 7. Cross-plot of $\delta^{34}\text{S}$ versus $\delta^{18}\text{O}_{\text{SO}_4}$ of groundwater, Messinian marls, cinerite, volcano-sedimentary rocks, and Messinian gypsum are from Grenade and Lorca [42] and Triassic sulfates from Apennines Italy [43], EM-Messinian marls, EM₁-volcanic products, EM₂-surface waters.

5. Conclusions

Interpretations of $\delta^{34}\text{S}$ and $\delta^{18}\text{O}$ values measured in groundwater samples indicate a dominant role of dissolved Messinian evaporites in the history of groundwater and argue against marine saltwater contamination of the groundwater. However, the primary seawater isotopic signature of evaporites deposited during the MSC, is affected by isotopic contributions from continental waters and volcanic products during the Neogene. Additionally, the differences observed in the isotopic composition between Messinian marls and groundwater in all aquifer samples, supports the hypothesis that salinization in groundwater is a consequence of contributions from MSC evaporites. The $\delta^{18}\text{O}$ and $\delta^2\text{H}$ isotope data obtained in this study show that for water samples from wells, their values do not generally lie along the GMWL and demonstrates that rapid isotopic enrichment can occur as a result of evaporation in this arid setting. Considering the high concentration of NO_3^- , actually, groundwaters in all aquifers undergo depletion due to anthropogenic sources, mainly agriculture and wastewater. Future geological and isotopic research would help further establish this proposed origin for groundwater salinization.

Author Contributions: Conceptualization, M.E. (Mohammed Elgettafi) and J.M.L.; methodology, M.E. (Mohammed Elgettafi) and M.H.; software, M.E. (Malak Elmeknassi); validation, A.C., A.E. and M.H.; investigation, M.E. (Mohammed Elgettafi), M.E. (Malak Elmeknassi) and A.E.; data curation, M.E. (Mohammed Elgettafi); writing original draft preparation, M.E. (Mohammed Elgettafi); writing—review and editing, J.M.L.; visualization, A.E. and M.H.; supervision, A.C. All authors have read and agreed to the published version of the manuscript.

Funding: This research received an external funding from the Spanish Agency of International Cooperation for the Development (AECID): Project CGL2009-07025.

Institutional Review Board Statement: Not applicable.

Informed Consent Statement: Not applicable.

Data Availability Statement: The data presented in this study are available to readers without any request from the corresponding author.

Acknowledgments: The present work is granted by the Spanish Agency of International Cooperation for the Development (AECID). The project has been funded by the Spanish Ministry of Science and Innovation through the project CGL2009-07025. The authors greatly appreciate the analytical support of the Scientific-Technical Services of the University of Barcelona and H. Bao at Louisiana State University.

Conflicts of Interest: The authors declare no conflict of interest.

References

- Bouchaou, L.; Choukr-Allah, R.; Hirich, A.; Ennasr, M.S.; Malki, M.; Abahous, H.; Bouaakaz, B.; Nghira, A. Climate change and water valuation in Souss-Massa region: Management and adaptive measures. *European Water* **2017**, *60*, 203–209.
- Hssaisoune, M.; Bouchaou, L.; Sifeddine, A.; Bouimetarhan, I.; Chehbouni, A. Moroccan Groundwater Resources and Evolution with Global Climate Changes. *Geosciences* **2020**, *10*, 81. [\[CrossRef\]](#)
- Elgettafi, M.; Himi, M.; Elmandour, A.; Casas, A.; Boubker, E. Messinian salinity crisis impact on the groundwater quality in Kert aquifer NE Morocco: Hydrochemical and statistical approaches. *Int. J. Water Res. Environ. Eng.* **2012**, *11*, 339–351.
- Hssaisoune, M.; Bouchaou, L.; Matsumoto, T.; Araguas, L.; Kraml, M.; Aggarwal, P. New evidences on groundwater dynamics from the Souss-Massa system (Morocco): Insights gained from dissolved noble gases. *App. Geochem.* **2019**, *109*, 104395. [\[CrossRef\]](#)
- Danni, S.O.; Bouchaou, L.; Elmouden, A.; Ait-Brahim, Y.; N'Da, B. Assessment of water quality and nitrate source in the Massa catchment (Morocco) using $\delta^{15}\text{N}$ and $\delta^{18}\text{O}$ tracers. *Appl. Radiat. Isot.* **2019**, *154*, 108859. [\[CrossRef\]](#)
- Re, V.; Sacchi, E.; Mas-Pla, J.; Menció, A.; El Amrani, N. Identifying the effects of human pressure on groundwater quality to support water management strategies in coastal regions: A multi-tracer and statistical approach (Bou-Areg region, Morocco). *Sci. Total Environ.* **2014**, *500*, 211–223. [\[CrossRef\]](#)
- Himi, M.; Tapias, J.; Benabdellouahab, S.; Salhi, A.; Rivero, L.; Elgettafi, M.; El Mandour, A.; Stitou, J.; Casas, A. Geophysical characterization of saltwater intrusion in a coastal aquifer: The case of Martil-Alila plain (North Morocco). *J. Afr. Earth Sci.* **2017**, *126*, 136–147. [\[CrossRef\]](#)
- Elgettafi, M.; Elmandour, A.; Himi, M.; Casas, A. The use of environmental markers to identify groundwater salinization sources in a Neogene basin, Kert aquifer case, NE Morocco. *Int. J. Environ. Sci. Technol.* **2013**, *10*, 719–728. [\[CrossRef\]](#)
- Karroum, M.; Elgettafi, M.; Elmandour, A.; Wilske, C.; Himi, M.; Casas, A. Geochemical processes controlling groundwater quality under semi-arid environment: A case study in central Morocco. *Sci. Total Environ.* **2017**, *609*, 1140–1151. [\[CrossRef\]](#)
- Chafouq, D.; El Mandour, A.; Elgettafi, M.; Himi, M.; Chouikri, I.; Casas, A. Hydrochemical and isotopic characterization of groundwater in the Ghis-Nekor plain (northern Morocco). *J. Afr. Earth Sci.* **2018**, *139*, 1–13. [\[CrossRef\]](#)
- Elmeknassi, M.; Bouchaou, L.; Elmandour, A.; Elgettafi, M.; Himi, M.; Casas, A. Multiple stable isotopes and geochemical approaches to elucidate groundwater salinity and contamination in the critical coastal zone: A case from the Bou-Areg and Gareb aquifers (North-Eastern Morocco). *Environ. Pollut.* **2022**, *300*, 118942. [\[CrossRef\]](#) [\[PubMed\]](#)
- Morel, J.L. Etats de contrainte et cinématique de la chaîne rifaine (Maroc) du Tortonien à l'actuel. *Geodin. Acta* **1989**, *3*, 283–294. [\[CrossRef\]](#)
- AitBrahim, L.; Chotin, P. Genèse et déformation des bassins néogènes du Rif central (Maroc) au cours du rapprochement Europe-Afrique. *Geodin. Acta* **1989**, *3*, 295–304. [\[CrossRef\]](#)
- Hsü, K.J.; Cita, M.B.; Ryan, W.B.F. *The Origin of the Mediterranean Evaporites*; Initial Reports of the Deep Sea Drilling Project; U.S. Government Printing Office: Washington, DC, USA, 1973; pp. 1203–1231.
- Montadert, L.; Sancho, J.; Fail, J.P.; Debyser, J.; Winnock, E. De l'âge tertiaire de la série salifère responsable des structures diapiriques en Méditerranée Occidentale (NordEst des Baléares). *Comptes Rendus l'Académie Sci.* **1970**, *271*, 812–815.
- Decima, A.; Wezel, F.C. Late Miocene Evaporites of the Central Sicilian Basin, Italy. *Initial. Rep. Deep. Sea Drill. Proj.* **1973**, *13*, 1234–1241.
- Clauzon, G.; Suc, J.P.; Gautier, F.; Berger, A.; Loutre, M.-F. Alternate interpretation of the Messinian Salinity Crisis: Controversy resolved? *Geology* **1996**, *24*, 363–366. [\[CrossRef\]](#)
- Krijgsman, W.; Langereis, C.G.; Zachariasse, W.J.; Boccaletti, M.; Moratti, G.; Gelati, R.; Iaccarino, S.; Papani, G.; Villa, G. Late Neogene evolution of the Taza-Guercif Basin (Rifian Corridor, Morocco) and implications for the Messinian salinity crisis. *Mar. Geol.* **1999**, *153*, 147–160. [\[CrossRef\]](#)
- García-Castellanos, D.; Villaseñor, A. Messinian salinity crisis regulated by competing tectonics and erosion at the Gibraltar arc. *Nature* **2011**, *480*, 359–363. [\[CrossRef\]](#)

20. Manzi, V.; Gennari, R.; Hilgen, F.; Krijgsman, W.; Lugli, S.; Roveri, M.; Sierro, F.J. Age refinement of the Messinian salinity crisis onset in the Mediterranean. *Terra Nova* **2013**, *25*, 315–322. [[CrossRef](#)]
21. Pérez-Asensio, J.N.; Aguirre, J.; Jimenez-Moreno, G.; Schmiedl, G.; Civis, J. Glacioeustatic control on the origin and cessation of the Messinian salinity crisis. *Glob. Planet. Chang* **2013**, *111*, 1–8. [[CrossRef](#)]
22. Lourens, L.J.; Antonarakou, A.; Hilgen, F.J.; Van Hoof, A.A.M.; Vergnaud Grazzini, C.; Zachariasse, W.J. Evaluation of the Pliocene to early Pleistocene astronomical time scale. *Paleoceanography* **1996**, *11*, 391–413. [[CrossRef](#)]
23. Baksi, A.K. A geomagnetic polarity timescale for the period 0–17Ma, based on ⁴⁰Ar/³⁹Ar plateau ages for selected field reversals. *Geophys. Res. Lett.* **1993**, *20*, 1607–1610. [[CrossRef](#)]
24. Do Couto, D. Evolution Géodynamique de la Mer D'alboran par L'étude des Bassins Sédimentaires. Ph.D. Thesis, Université Pierre et Marie Curie, Paris, France, 2014.
25. El Azzouzi, M.; Bernard-Griffiths, J.; Bellon, H.; Maury, R.C.; Pique, A.; Fourcade, S.; Cotten, J.; Hernandez, J. Evolution des sources du volcanisme marocain au cours du Neogene. *CR Acad. Sci. Paris* **1999**, *329*, 95–102. [[CrossRef](#)]
26. D'Acremont, E.; Gutscher, M.A.; Rabaute, A.; Mercier de Lépinay, B.; Lafosse, M.; Poort, J.; Ammar, A.; Tahayt, A.; Le Roy, P.; Smit, J.; et al. High-resolution imagery of active faulting offshore Al Hoceima, Northern Morocco. *Tectonophysics* **2014**, *632*, 160–166. [[CrossRef](#)]
27. El Alami, S.O.; Tadili, B.A.; Cherkaoui, T.E.; Medina, F.; Ramdani, M.; AitBrahim, L.; Harnaff, M. The Al Hoceima earthquake of May 26, 1994 and its aftershocks: A seismotectonic study. *Ann. Geofis.* **1998**, *41*, 519–537. [[CrossRef](#)]
28. Medina, F.; El Alami, S.O. Focal mechanisms and state of stress in the Al Hoceima area (Central Rif, Morocco). *Bull. l'Inst. Rabat Sect. Sci. Terre* **2006**, *28*, 19–30.
29. Poujol, A.; Ritz, J.F.; Tahayt, A.; Vernant, P.; Condomines, M.; Blard, P.H.; Billant, J.; Vacher, L.; Tibari, B.; Hni, L.; et al. Active tectonics of the northern Rif (Morocco) from geomorphic and geochronological data. *J. Geodyn.* **2014**, *77*, 70–88. [[CrossRef](#)]
30. Elmandour, A.; El Yaouti, F.; Fakir, Y.; Zarhloule, Y.; Benavente, J. Evolution of groundwater salinity in the unconfined aquifer of BouAreg, Northeastern Mediterranean coast, Morocco. *Environ. Geol.* **2008**, *54*, 491–503. [[CrossRef](#)]
31. El Yaouti, F.; Elmandour, A.; Khattach, D.; Benavente, J.; Kaufmann, O. Salinization processes in the unconfined aquifer of Bou-Areg (NE Morocco): A geostatistical, geochemical, and tomographic study. *Appl. Geochem.* **2009**, *24*, 16–31. [[CrossRef](#)]
32. Frizon de Lamotte, D. La Structure du Rif Oriental (Maroc): Rôle de la Tectonique Longitudinale et Importance Des Fluides. Ph.D. Thesis, University of Pierre et Marie Curie, Paris, France, 1985.
33. Elgettafi, M. Caractérisation des Processus de la Salinisation des Eaux Souterraines de la Plaine de Kert, Maroc, Nord Oriental: Approches Hydrogéologique, Géochimique et Géophysique. Ph.D. Thesis, Université de Marrakech, Marrakech, Morocco, 2011.
34. Carlier, P. *Carte Hydrogéologique au 1/50,000 de la Plaine du Moyen-Kerte, Province de Nador, Maroc Nord-Oriental: Notice Explicative*; Éditions du Service Géologique du Maroc: Rabat, Morocco, 1973; Volume 250.
35. Craig, H. Isotopic variation in meteoric waters. *Science* **1961**, *133*, 1702–1703. [[CrossRef](#)]
36. Gamsjäger, H.; Murmann, R.K. *Advances in Inorganic and Bioinorganic Mechanisms*; Sykes, A.G., Ed.; Academic Press: London, UK, 1983; Volume 2, pp. 317–381.
37. Boschetti, T.; Iacumin, P. Continuous-flow $\delta^{18}\text{O}$ measurements: New approach to standardization, high-temperature thermodynamic and sulfate analysis. *Rapid Commun. Mass Spectrom.* **2005**, *19*, 3007–3014. [[CrossRef](#)] [[PubMed](#)]
38. Van Stempvoort, D.R.; Krouse, H.R. Controls of $\delta^{18}\text{O}$ in sulfate: Review of experimental data and application to specific environments. *Environ. Geochem. Sulfide Oxid.* **1994**, *29*, 446–480.
39. Elkilany, A. Hydrologie et Cycles Biogéochimiques du Soufre Dans Deux Bassins Marginaux de Méditerranée Pendant la Crise de Salinité Messinienne. Ph.D. Thesis, Sorbonne University, Paris, France, 2018.
40. Claypool, G.E.; Holser, W.T.; Kaplan, I.R.; Zak, I. The age curves of sulfur and oxygen isotope in marine sulfate and their mutual interpretations. *Chem. Geol.* **1980**, *28*, 199–260. [[CrossRef](#)]
41. Urresti-Estala, B.; Vadillo-Pérez, I.; Jiménez-Gavilan, P.; Soler, A.; Sanchez-García, D.; Carrasco-Cantos, F. Application of stable isotopes ($\delta^{34}\text{S-SO}_4$, $\delta^{18}\text{O-SO}_4$, $\delta^{15}\text{N-NO}_3$, $\delta^{18}\text{O-NO}_3$) to determine natural background and contamination sources in the Guadalhorce River Basin (southern Spain). *Sci. Total Environ.* **2015**, *506*, 46–57. [[CrossRef](#)] [[PubMed](#)]
42. Pierre, C. Teneurs en Isotopes Stables (¹⁸O, ²H, ¹³C, ³⁴S) et Conditions de Genèse des Evaporites Marines: Application à Quelques Milieux Actuels et au Messinien de la Méditerranée. Ph.D. Thesis, University of Paris-Sud, Orsay, France, 1982; 226p.
43. Boschetti, T.; Cortecchi, G.; Toscani, L.; Iacumin, P. Sulfur and oxygen isotope compositions of Upper Triassic sulfates from Northern Apennines (Italy): Palaeogeographic and hidrogeochemical implications. *Geol. Acta* **2011**, *9*, 129–147.